

The Area Coverage of Geophysical Fields as a Function of Sensor Field-of-View

Jeffrey R. Key*

In many remote sensing studies of geophysical fields such as clouds, land cover, or sea ice characteristics, the fractional area coverage of the field in an image is estimated as the proportion of pixels that have the characteristic of interest (i.e., are part of the field) as determined by some thresholding operation. The effect of sensor field-of-view on this estimate is examined by modeling the unknown distribution of subpixel area fraction with the beta distribution, whose two parameters depend upon the true fractional area coverage, the pixel size, and the spatial structure of the geophysical field. Since it is often not possible to relate digital number, reflectance, or temperature to subpixel area fraction, the statistical models described are used to determine the effect of pixel size and thresholding operations on the estimate of area fraction for hypothetical geophysical fields. Examples are given for simulated cumuliform clouds and linear openings in sea ice, whose spatial structures are described by an exponential autocovariance function. It is shown that the rate and direction of change in total area fraction with changing pixel size depends on the true area fraction, the spatial structure, and the thresholding operation used.

INTRODUCTION

An analytical description of the relationship between the satellite-derived fractional area coverage of a geophysical field and sensor resolution is needed in order to assess the potential error in many satellite-derived products and to understand in a more quantitative man-

ner the benefits of different sensor systems. While there have been studies of the effect of sensor resolution on parameter retrieval, the approaches have been empirical and specific to a single geophysical variable. In the analysis of land cover classes, for example, the variance within satellite images has been examined as a function of measurement scale for the purpose of determining the optimal resolution for change monitoring (e.g., Woodcock and Strahler, 1987; Townshend and Justice, 1988). In studies of cloud fraction, real and synthetic data containing cloud fields were degraded in resolution, and the fractional coverage was observed as a function of scale (e.g., Wielicki and Parker, 1992; Wielicki and Welch, 1986; Shenk and Salomonson, 1972).

Even though these studies are useful, no concise statement of the relationship between fractional coverage and sensor resolution has been given, so that the results are difficult to generalize to other geophysical fields. A complete analytical description of the problem is difficult at best, involving geometrical (viewing geometry), spectral (band location and width), radiometric (signal-to-noise ratio, quantization levels), and spatial (sensor resolution or pixel size) properties. In this article, a first attempt at an analytical approach to the problem is described. We are concerned only with the fraction of the image area covered by some geophysical parameter, for example, cloud or open water fraction. We take an approach similar to that of Shenk and Salomonson (1972), where cloud fields were simulated and the relationship between pixel size, cloud size, estimated area fraction, and true area fraction were expressed for different thresholding operations. That work is extended, however, by generalizing the problem to any geophysical variable whose spatial structure can be described by its autocovariance function. Additionally, a specific probability density function is used as a model of the subpixel area fraction so that the results do not depend upon a given simulation. In this manner the results are applicable to a wide variety of geophysical

*Cooperative Institute for Research in Environmental Sciences, Division of Cryospheric and Polar Processes, University of Colorado, Boulder

Address correspondence to Jeffrey R. Key, CIRES, Univ. of Colorado, Campus Box 449, Boulder, CO 80309-0449.

Received 30 September 1992; revised 8 January 1994.

fields including clouds, sea ice fractures ("leads"), and land cover classes. In the next section the analytical approach is described. The models are then applied to simulated fields of clouds and sea ice leads in a satellite image context.

ANALYTICAL APPROACH

Our goal is to determine the proportion of pixels in an image that have the characteristic of interest; for example, the fraction that are cloudy or that are sea ice leads, etc., given some thresholding operation. This depends on the distribution of the subpixel area fraction, which is specified by its shape, mean, and variance. The variance depends on the pixel size and the spatial structure of the geophysical parameter, described by its autocovariance function. The formalization that follows can be applied to virtually any geophysical parameter whose spatial distribution can be described in this manner.

Indicator Function

Let $q(\mathbf{x})$ be a measurable property (e.g., temperature or reflectance) at a point whose position is represented by the location vector \mathbf{x} , and define ζ to be any condition on q . For example, ζ might be the condition $q(\mathbf{x}) < T_s - \delta$, where T_s is the surface temperature and δ is some threshold amount. The indicator function $I(\mathbf{x})$ in a square region R is equal to 1 if $q(\mathbf{x})$ satisfies ζ and 0 otherwise. The fractional coverage for which q satisfies ζ is given by

$$P = A_R^{-2} \int_R I(\mathbf{x}) d\mathbf{x}, \quad (1)$$

where A_R is the side length of R and is a normalizing factor. For the rest of the discussion R is a satellite image. The probability density function (pdf) of I is $f_I(1) = P$ and $f_I(0) = 1 - P$.

Now let $q_z(\mathbf{y})$ be a measurable property of a pixel Z within R centered at location \mathbf{y} (again, a vector). As measured by the sensor, q_z would be an average over a pixel:

$$q_z(\mathbf{y}) = A_z^{-2} \int_{Z(\mathbf{y})} q(\mathbf{x}) d\mathbf{x},$$

where A_z is the side length of the pixel. An argument could be made for using the sensor point spread (transfer) function, but for simplicity a rectangular spatial response is assumed. The fractional area of R for which q_z satisfies ζ is an estimate of the true fractional coverage and is

$$P' = N^{-1} \sum_R I_z(\mathbf{y}), \quad (2)$$

where N is the number of pixels in R and I_z is the indicator function for the pixel based on q_z , defined in the same way as is I (for a point) based on q . Our goal is to relate P' to P over a range of A_z .

To determine P' analytically, the probability density of I_z must be known. It is not trivial, and depends on P , ζ , pixel size, and the way in which objects satisfying ζ are distributed in space. Since I_z is a function of q_z , which in turn depends on the fractional coverage within a pixel p_z , then (under certain conditions) I_z can be expressed in terms of p_z . For example, consider a cloud pattern where the cloud top temperature T_c is everywhere the same and is less than the surface temperature T_s . Let ζ be a thresholding operation such that

$$I_z = \begin{cases} 1 & \text{if } q_z < T_s - \delta, \\ 0 & \text{otherwise,} \end{cases}$$

where δ is some threshold amount. This is equivalent to

$$I_z = \begin{cases} 1 & \text{if } p_z \geq p, \\ 0 & \text{otherwise.} \end{cases} \quad (3)$$

The expression $p_z \geq p$ states that the fractional coverage within the pixel is greater than some quantity p , which in this example has a value such that

$$(1 - p)T_s + pT_c < T_s - \delta.$$

In reality there may be a distribution of T_c , although we do not address this issue here. So, based on Eq. (3), the probability density of I_z is

$$\begin{aligned} f_{I_z}(1) &= \text{Prob}(P_z \geq p), \\ f_{I_z}(0) &= \text{Prob}(P_z < p) = 1 - f_{I_z}(1), \end{aligned}$$

where P_z represents the random variable subpixel fractional coverage (with specific realization p_z), and $\text{Prob}(P_z \geq p)$ represents the probability that the fractional coverage within the pixel is greater than some quantity p . Now, how is $\text{Prob}(P_z \geq p)$ determined?

Distribution of Subpixel Area Coverage

For a single pixel the fractional coverage of the geophysical parameter is

$$p_z(\mathbf{y}) = A_z^{-2} \int_{Z(\mathbf{y})} I(\mathbf{x}) d\mathbf{x},$$

which can be used as an estimate of the true area fraction in the image P . After Stoyan et al. (1989, p. 184), the expected value and variance of P_z are

$$\begin{aligned} \mu &= E(P_z) = P, \\ \sigma^2 &= \text{Var}(P_z) = E[P_z - E(P_z)]^2 \\ &= E\left\{ \left[A_z^{-2} \int_Z I(\mathbf{x}) d\mathbf{x} - P \right] \right. \\ &\quad \left. \times \left[A_z^{-2} \int_Z I(\mathbf{x}') d\mathbf{x}' - P \right] \right\} \\ &= A_z^{-4} \int_Z \int_Z k_r(|\mathbf{x} - \mathbf{x}'|) d\mathbf{x} d\mathbf{x}', \end{aligned} \quad (4)$$

where k_r is the autocovariance function for the indicator

function. The effect of pixel size on the autocovariance function has been studied by Jupp et al. (1988; 1989), although the autocovariance function in (5) does not depend on pixel size; that is, it refers to the true underlying (point) autocovariance. The expression (5) for the variance of the subpixel area fraction can be expanded as

$$\sigma^2 = A_z^{-4} \int_0^{A\sqrt{2}} k_i(r)r\{A^2[2\pi - 8\xi(r)] - 8Ar\sqrt{2} \cos[\pi/4 + \xi(r)] + 2r^2 \cos[2\xi(r)]\} dr, \quad (6)$$

where

$$\xi(r) = \begin{cases} 0, & 0 \leq r \leq A \\ 1/4 \cos^{-1}[1 + 2/(\sqrt{2} - 1)](1 - r/A), & A < r \leq A\sqrt{2}, \end{cases}$$

as given in Rothrock and Thorndike (1984), with a correction made here. This applies to a square pixel and an isotropic covariance function.

If a specific model distribution for P_z is assumed, with expected value and variance as defined above, then the density of the pixel indicator function is also known. Here we use the Beta distribution, a two-parameter density function defined over the closed interval $0 \leq p \leq 1$ that is often used as a model for proportions:

$$f_\beta(p) = \begin{cases} p^{\gamma-1}(1-p)^{\beta-1} \frac{\Gamma(\gamma+\beta)}{\Gamma(\gamma)\Gamma(\beta)}, & \gamma, \beta > 0, 0 \leq p \leq 1, \\ 0, & \text{elsewhere.} \end{cases}$$

The two parameters can be determined by maximum likelihood estimation based on the mean and variance of the subpixel fractional coverage in Eqs. (4) and (5) (Falls, 1974):

$$\beta = \frac{1-\mu}{\sigma^2} [\mu(1-\mu) - \sigma^2],$$

$$\gamma = \frac{\mu\beta}{1-\mu}.$$

The shape of the distribution is related to the size of the pixel relative to the spatial structure (e.g., wavelength) of the geophysical parameter. In the limiting case with very large pixels relative to the wavelength of cloud elements, for example, most pixels would have a similar subpixel cloud fraction and the variance would be very small. The distribution would therefore have a single peak. On the other hand, if the pixel size is very small, then the likelihood of pixels being either completely overcast or completely clear increases, the variance of the subpixel area fraction increases, and two peaks are expected. This is illustrated in Figure 1 where the beta distribution is shown for a mean area fraction of 0.2 and variances of 0.1, 0.05, and 0.01.

The beta distribution has often been used to describe cloud amount frequency distributions (e.g., Falls, 1974; Henderson-Sellers and McGuffie, 1992; Jones,

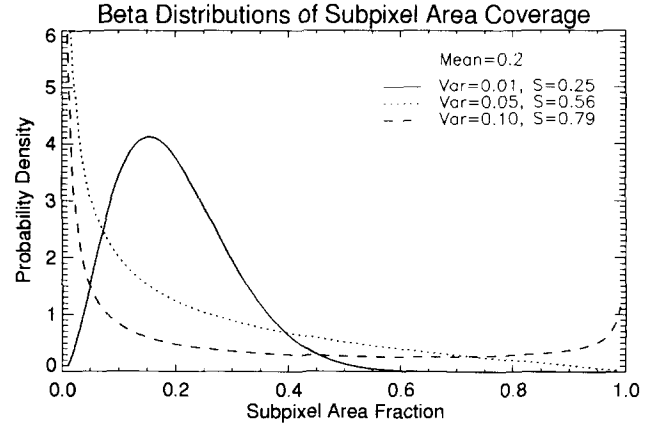


Figure 1. Three realizations of the Beta probability density function for a mean subpixel fractional coverage of 0.2 and three different variances. The shape parameter S is also given.

1992). More recently a similar distribution, the Burger distribution, has also been used (e.g., Henderson-Sellers and McGuffie, 1992). The Burger distribution is described by the mean cloud amount and a correlation distance defined as the separation distance between pixels at which the autocorrelation drops below 0.99. Correlation distance was also used by Gringorten (1979), who developed models through simulations describing the probability of a meteorological condition occupying some fraction of a line or area.

Jones (1992) presents a shape parameter that can be used to describe the beta distribution. It is defined as

$$S = \sigma / [\mu(1-\mu)]^{1/2}.$$

$S > 0.6$ implies a U-shaped distribution, $S \approx 0.6$ implies a flat distribution, and $S < 0.6$ implies a distribution with a central peak. Values of the shape parameter are also shown in Figure 1. In the examples that follow, and in most satellite remote sensing applications where pixel sizes are 1 km or less, $S > 0.6$.

Changes in Total Area Fraction

Now we return to the estimate of the total area fraction in an image, P' , which is the proportion of pixels in the image for which the indicator function takes on a value of 1, as defined in Eq. (2). Given the distribution of subpixel area fraction described here by the beta pdf, P' is simply $\text{Prob}(P_z \geq p)$ or the probability that the subpixel area fraction is greater than some threshold value p . This is the area under the curve to the right of any given value along the horizontal axis in Figure 1.

Figure 2 shows the estimated total area fraction for four true area fractions as a function of the subpixel area fraction variance (along the abscissa) and the threshold value. The variance and the true area fraction together define the distribution of subpixel area fraction so that

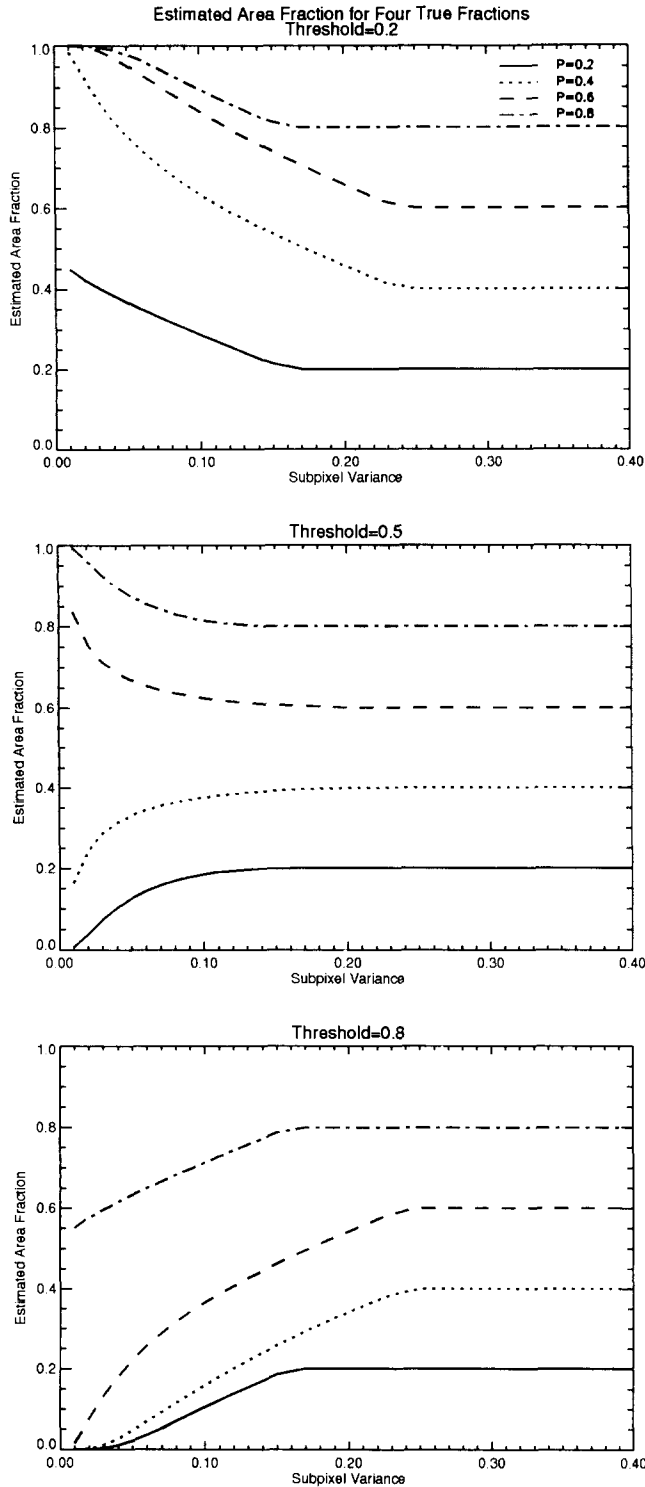


Figure 2. Estimated total area fraction as a function of the subpixel area fraction variance and true area fraction. Results for three subpixel area fraction thresholds are shown.

a wide range of spatial structures and pixel sizes is represented in the three plots, independent of any particular geophysical field. For a given autocovariance function, pixel size decreases toward the right in the

plots. Note that there is an upper limit on the variance, defined by the point at which the two parameters of the beta distribution are equal to or less than 0. This point is $\mu - \mu^2$. In theory, decreasing the pixel size (increasing the variance) beyond this point has no effect on the estimate of the total area fraction.

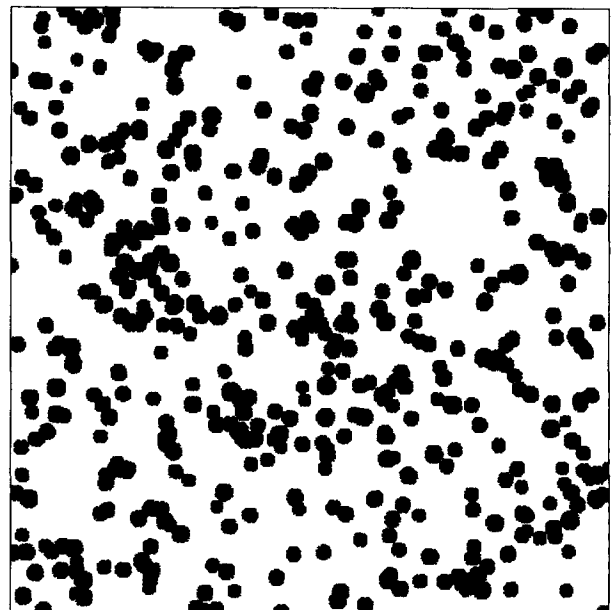
APPLICATION

In this section the above models are applied to simulated satellite data. Since these models require some *a priori* knowledge of the field's spatial structure, they cannot be used to assess the error in the total area fraction estimate from a single image alone. Instead, this section illustrates how the error can be assessed for typical realizations of two very different geophysical variables: clouds and sea ice leads.

A cloud field is simulated as a distribution of disks whose center locations follow a binomial point process and whose diameters are approximately normally distributed (in a true Gaussian distribution, negative diameters would be possible). One realization is shown in Figure 3, where the mean diameter is 2000 m. Sea ice leads are modeled as a Poisson line process. The mean spacing between the lines (leads) is 3000 m, and their orientations are random. The lines are assigned thicknesses (widths) following the negative exponential density function:

$$f_w(w) = \frac{1}{\lambda} e^{-w/\lambda}$$

Figure 3. A simulated cloud field, where cloud centers follow a binomial point process and cloud diameters are Gaussian-distributed.



where w is lead width and λ is the mean width. For the simulations $\lambda = 200$ m. One realization is shown in Figure 4.

To examine the effects of pixel size on the estimated fractional area coverage, these images were degraded by simple averaging of 2×2 pixel cells. Four degradations were performed. Initial pixel size is 50 m; pixel size doubles with each degradation so that the largest pixel examination is 800 m.

Exponential covariance is a reasonable model for many geophysical parameters and is used here:

$$k_i(r) = P(1 - P)e^{-ar}, \quad r, a \geq 0, \quad (7)$$

where a describes the dependence of the covariance on the separation distance r . Implicit in this expression is that $q(x)$ is isotropic. Using Eq. (7) and Eq. (6) gives

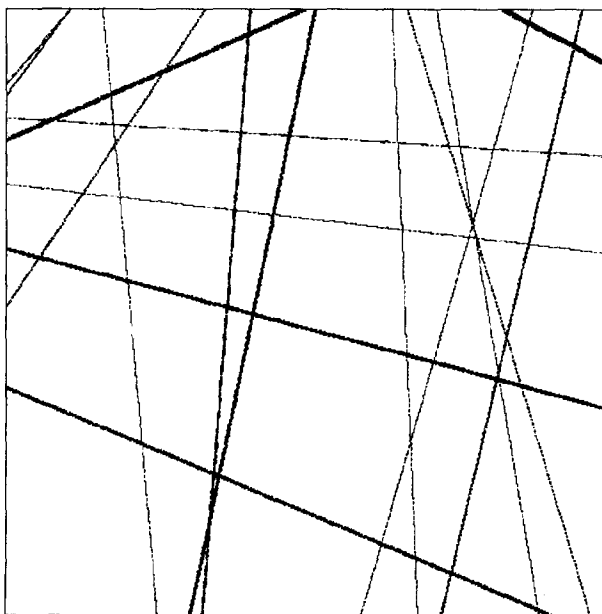
$$\sigma^2 = P(1 - P)A_z^{-4} \int_0^{A\sqrt{2}} e^{-ar} r \{ A^2 [2\pi - 8\xi(r)] - 8Ar\sqrt{2} \cos[\pi/4 + \xi(r)] + 2r^2 \cos[2\xi(r)] \} dr. \quad (8)$$

Note that the effects of area coverage and autocovariance (e.g., the size of objects and pixel size) separate out:

$$\sigma^2/P(1 - P) = f(A),$$

which is essentially Jones's (1992) shape parameter S . This is not strictly true for the correlation functions of the cloud and lead models employed here, but is still useful for the purposes of this article. The parameter

Figure 4. A Poisson line process, used to stimulate linear openings in sea ice.



a in (7) and (8) can be determined from observed autocovariances by rewriting (7) in linear form,

$$\ln[k_i(r)] = \ln[P(1 - P)] - ar, \quad (9)$$

and solving by least squares regression. For the applications below, the parameter a is determined for three evenly spaced, parallel transects in the imagery and then averaged.

Table 1 illustrates the application of the beta distribution and its estimated moments to the synthetic data in Figures 3 and 4. Listed are the pixel size relative to the smallest pixel (where the smallest pixel is 1), a determined from the image, the "true" area fraction P determined from the highest resolution image in which each pixel is either empty or completely full, the observed variance of the subpixel fractional coverage P_z , and the variance of P_z estimated by solving Eq. (8) numerically. The difference in the a values for the two different fields reflects their spatial structures where the (auto)covariance of the synthetic leads falls off more rapidly than that of the clouds. The true area fraction and the observed and estimated variances in Table 1 for the cloud case were used to generate beta pdfs for comparison with the observed distribution of subpixel area fraction. The results are shown in Figure 5 as the complement of the cumulative probability distribution function. End effects are due to binning procedures. Shown this way, it is straightforward to determine the total fractional area coverage estimate P' of the image for any threshold. For example, in the top plot of Figure 5, any threshold greater than 0.1 (in theory, any value greater than 0) would yield the same cloud area fraction: 0.25. With a larger pixel size, however, this is not the case (Figure 5, bottom). A threshold of 0.2 produces a total area fraction of 0.33 while a threshold of 0.6 yields a total fraction of about 0.2.

DISCUSSION

Except in the case of a uniform target and background, as with a single cloud deck over open water, it will generally not be possible to determine the subpixel area fraction and hence to apply the models presented here.

Table 1. Relative Pixel Size, the Covariance Parameter, True Total Area Fraction, and the Observed and Estimated Variances of the Subpixel Area Fraction

Image	A	a	P	Observed Var (P_z)	Estimated Var (P_z) ^a
Clouds	1	0.05	0.246	0.185	0.178
	16			0.133	0.124
Leads	1	0.15	0.033	0.032	0.029
	16			0.010	0.011

^a Estimated using Eq. (8).

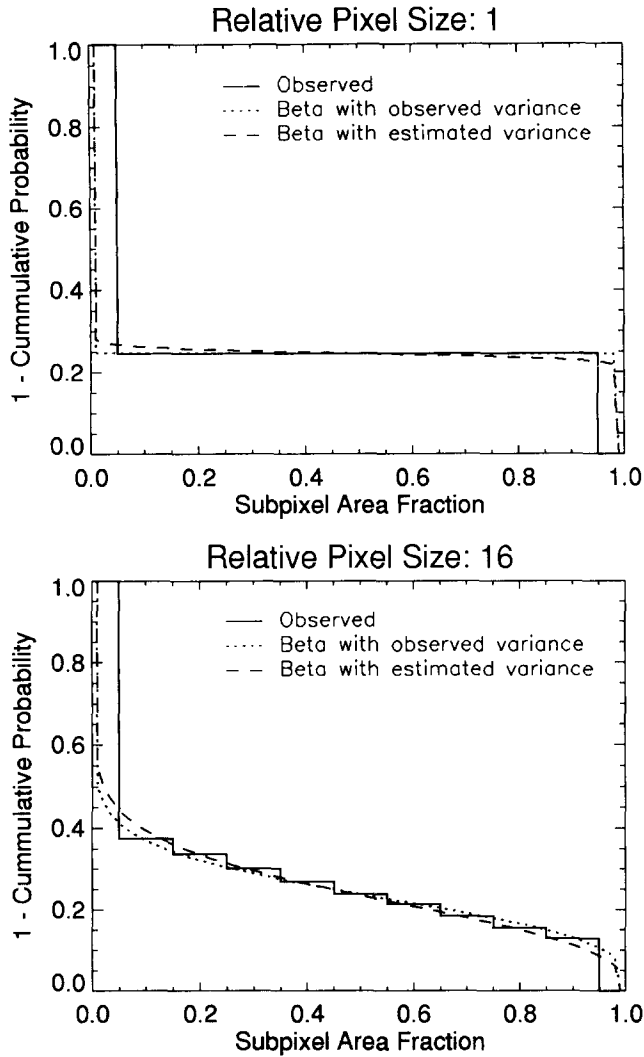


Figure 5. Complement of the cumulative probability function of subpixel area fraction for the cloud field in Figure 3, using two different relative pixel sizes. Shown are the observed and estimated distributions, where the estimated functions are based on the true total area fraction and the observed and estimated variances in subpixel area fraction (Table 1).

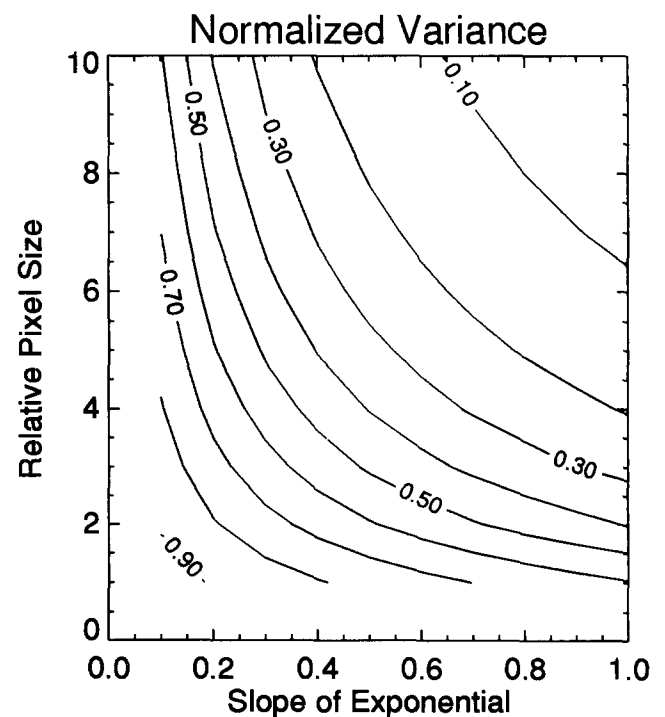
For example, suppose thermal data are being examined for the purpose of estimating cloud fraction. Even if the background (land or ocean) temperature is known, a small deviation from that temperature in a pixel could be caused by a small amount of very cold cloud or a large amount of cloud only slightly colder than the background, or numerous other combinations of cloud amount, cloud optical thickness, and cloud top temperature. The problem is that a single threshold in terms of subpixel area fraction P_z can translate into a range of temperature thresholds and vice versa. In theory, there is a single P_z threshold that would yield the same P' over a wide range of pixel sizes. This can be seen most readily in Figures 1 and 5. At the smallest pixel size

the distribution of p_z is bimodal so that a range of thresholds would yield the same, correct P' , that is, $P' = P$. At a large pixel size there may be only one correct threshold, but it is within the range found for the small pixel case. When dealing with DNs (temperatures, reflectances, etc.), however, this may not be the case. Further research is needed concerning the effect of "regularization," or the averaging over the point spread function of sensors. The work of Jupp et al. (1988; 1989) is important in this regard.

Given the pixel unmixing problem when the spectral structure of the field is complex, one way (perhaps the only way at present) to relate the DN threshold to the subpixel area fraction threshold is to choose a DN threshold very close to the background value. This is analogous to choosing a small subpixel area fraction threshold, as in the top plot of Figure 2. If the pixel size is small enough relative to the spatial structure of the field, then P' will be a good estimate of P . If the pixel is not small, then all that can be said is that $P' \geq P$ (see Figure 2, top). How small is small?

To more easily address this and similar questions, Figure 6 was constructed as an aid in the interpretation of (8). The figure shows the normalized variance as a function of relative pixel size A and the slope of the

Figure 6. The variance of the distribution of subpixel area fraction computed from Eq. (8), normalized by $P(1 - P)$, as a function of relative pixel size and the slope of the exponential covariance function α . To determine the actual variance, the contour value must be multiplied by $P(1 - P)$.



exponential covariance function α . The normalization was done by computing Eq. (8) without the $P(1-P)$ term so as to remove the dependence on P . Therefore, to use this figure, the reported values must be multiplied by this term to retrieve the actual variance of the subpixel area fraction distribution. The two important relationships in Eq. (8) that are illustrated in Figure 6 are that an increase in the pixel size or an increase in the rate at which the covariance drops off with distance both result in a decreasing variance. Not shown in Figure 6 but implicit in (8) is the relationship between P and the variance: the variance of P_z is maximum when $P=0.5$ for a constant A and α .

Now, if we interpret the previous condition that a DN threshold close in value to that of the background translates into a subpixel area fraction threshold of approximately 0.2 (for the purpose of illustration), then Figures 2 and 6 can be used together to answer "what if" questions. For example, suppose that the geophysical field had an exponential autocovariance with $\alpha = 0.4$ and the true area fraction is 0.2. What would be the estimated total area fraction P' with a relative pixel size of 2? The variance based on Figure 6 would then be approximately 0.11 and from Figure 2 the estimated area fraction would be about 0.28 with a threshold of 0.2, 0.19 with a threshold of 0.5, and 0.12 with a threshold of 0.8. With a relative pixel size of 6, the variance is 0.056 and the area fraction estimates are 0.36, 0.13, and 0.02, respectively.

It should be noted that in theory a beta distribution that is consistent with the observed autocovariance function can be chosen. The regression method of estimating the rate of decay of the autocovariance described by Eq. (9) also provides an estimate of P . From these two parameters the variance in Eq. (8) is then determined, thereby defining the beta distribution. However, the autocovariance is affected by pixel size, as described in Jupp et al. (1988; 1989). Therefore, the autocovariance determined by Eq. (9) must be translated into the "true" (point) autocovariance before the correct beta distribution can be determined.

SUMMARY AND CONCLUSIONS

In most analyses of geophysical fields in satellite imagery each pixel is eventually labeled as either containing or not containing the variable of interest. This labeling is accomplished through a thresholding operation, where pixels whose DN is different from the background DN by more than some threshold amount are labeled as being part of the geophysical field. Estimates of the area coverage of the field are obtained as the proportion of these pixels in the image. The actual subpixel area fraction (P_z) of the geophysical field varies considerably, however, as a function of the true area fraction, the spatial structure, and the pixel size. It has been shown

here that the beta distribution is an adequate model of the distribution of P_z . In the simple case of a uniform target (e.g., a cloud deck) and a uniform background, the DN thresholding operation can be described in terms of a subpixel area fraction threshold. The estimate of the total area fraction within an image is then the probability of obtaining a subpixel amount greater than the threshold, which can be easily determined from the beta distribution.

The statistical models presented allow us to answer many questions in a hypothetical sense about the effect of spatial structure, pixel size, and thresholding operations on the estimated fractional area coverage in an image. It should be clear from the results presented here that the thresholding approach can result in substantial errors. Of course, if the subpixel area fraction were known, then there would be no need for employing the threshold procedure. Unfortunately, geophysical fields are often complex so that the relationship between a DN threshold and a subpixel area fraction threshold is not clear. Additional research is needed in this area to define the effect of pixel size on the distribution of DNs (e.g., temperature, reflectance) in an image.

There are other approaches to the scaling problem that deserve mention. The basic idea of labeling pixels to estimate area fraction can be described by the set operations of erosion and dilation used in mathematical morphology (Serra, 1982). For example, pixels can be labelled as "hitting" an object if any part of the object is within the pixel and "not hitting" otherwise. This is analogous to thresholding near the background value. As the pixel size approaches the image size the estimated area fraction approaches unity. On the other hand, if a "hit" is defined to occur only if the pixel is completely inside an object, the estimated area fraction approaches zero as the pixel size increases.

Fractals have also been used to describe the relationship between area coverage and measurement scale. For example, in Cahalan and Joseph (1989) the relationship between cloud area and perimeter was described by a fractal scaling law for clouds. The scaling properties of stream channels have been described in terms of "fat" fractals (Karlinger and Troutman, 1992). Rainfall amounts have been studied as cascade processes (Gupta and Waymire, 1993). Unfortunately, these are all specific to a particular geophysical variable, and are difficult to generalize to remote sensing studies.

This work was supported by NASA Grants NAGW-2407 and NAGW-2598 and ONR Grant N00014-90-J-1840. Thanks are due to D. Jupp, T. Over, and S. Peckham for useful discussions, and to an anonymous reviewer for helpful suggestions. Mathematics was used for many of the numerical and symbolic computations.

REFERENCES

- Cahalan, R. F., and Joseph, J. H. (1989), Fractal statistics of cloud fields, *Monthly Wea. Rev.* 117(2):261–272.
- Falls, L. W. (1974), The beta distribution: a statistical model for world cloud cover, *J. Geophys. Res.* 79(9):1261–1264.
- Gringorten, I. I. (1979), Probability models of weather conditions occupying a line or area, *J. Appl. Meteorol.* 18:957–977.
- Gupta, V. K., and Waymire, E. C. (1993), A statistical analysis of mesoscale rainfall as a random cascade, *J. Appl. Meteorol.*, 32(2):251–267.
- Henderson-Sellers, A., and McGuffie, K. (1992), Investigation of the Burger distribution to characterize cloudiness, *J. Climate* 4:1181–1209.
- Jones, P. A. (1992), Cloud-cover distributions and correlations, *J. Appl. Meteorol.* 31(7):732–741.
- Jupp, D. L. B., Strahler, A. H., and Woodcock, C. E. (1988), Autocorrelation and regularization in digital images I. Basic theory, *IEEE Trans. Geosci. Remote Sens.* 26(4):463–473.
- Jupp, D. L. B., Strahler, A. H., and Woodcock, C. E. (1989), Autocorrelation and regularization in digital images II. Simple image models, *IEEE Trans. Geosci. Remote Sens.* 27(3):247–258.
- Karlinger, M. R., and Troutman, B. M. (1992), Fat fractal scaling of drainage networks from a random spatial network model, *Water Resources Res.* 28(7):1975–1981.
- Rothrock, D. A., and Thorndike, A. S. (1984), Measuring the sea ice floe size distribution, *J. Geophys. Res.* 89(C4):6477–6486.
- Serra, J. (1982). *Image Analysis and Mathematical Morphology*, Academic, London.
- Shenk, W. E., and Salomonson, V. V. (1972), A simulation study exploring the effects of sensor spatial resolution on estimates of cloud cover from satellites, *J. Appl. Meteorol.* 11:214–220.
- Stoyan, D., Kendall, W. S., and Mecke, J. (1989), *Stochastic Geometry and Its Applications*, Wiley, New York, 345 pp.
- Townshend, J. R. G., and Justice, C. O. (1988), Selecting the spatial resolution of satellite sensors required for global monitoring of land transformations, *Int. J. Remote Sens.* 9(2):187–236.
- Wielicki, B. A., and Parker, L. (1992), On the determination of cloud cover from satellite sensors: the effect of sensor spatial resolution, *J. Geophys. Res.* 97(D12):12,799–12,823.
- Wielicki, B. A., and Welch, R. M. (1986), Cumulus cloud properties derived using Landsat satellite data, *J. Clim. Appl. Meteorol.* 25:261–276.
- Woodcock, C. E., and Strahler, A. H. (1987), The factor of scale in remote sensing, *Remote Sens. Environ.* 21:311–316.